Magnetic Exciton Relaxation and Spin−Spin Interaction by the Time-Delayed Photoluminescence Spectra of ZnO:Mn Nanowires

Ruibin Liu, Lijie Shi, and Bingsuo Zou*

Beijing Key Lab of Nanophotonics and Ultrafine Optoeletronic Systems, Beijing Institute of Technology, Beijing 100081, China

ⓢ *Supporting Information*

ABSTRACT: ZnO:Mn nanostructures are important diluted magnetic materials, but their electronic structure and magnetic origin are still not well understood. Here we studied the time-delayed and power-dependent photoluminescence spectra of Mn(II) doped ZnO nanowires with very low Mn concentration. From the time-delayed emission spectra, we obtained their electronic levels of single Mn ion replacement of Zn ions in ZnO nanowire. The high d-level emissions show up unusually because of the stronger p−d hybridization than that in ZnS, as well as the spin−spin coupling. After increasing Mn doping concentration, the ferromagentic cluster of the Mn−O−Mn with varied configurations can form and give individual emission peaks, which are in good agreement with the ab initio calculations. The presence of clustered Mn ions originates from their ferromagnetic coupling. The lifetimes of these d levels show strong excitation power-dependent behavior, indication of strong spin-dependent coherent emission. One-dimensional structure is critical for this coherent emission behavior. These results indicate that the d state is not within Mn ion only, but a localized exciton magnetic polaron, Mn−O−Mn coupling should be one source of ferromagnetism in ZnO:Mn lattice, the latter also can combine with free exciton for EMP and produce coherent EMP condensation and emission from a nanowire. This kind of nanowires can be expected to work for both spintronic and spin-photonic devices if we tune the transition metal ion doping concentration in it.

Time delayed PL spectra unveil the electronic states of ZnO:Mn nanowire

Time-delayed photoluminescence spectra of ZnO:Mn nanowire by ns pulse excitation

KEYWORDS: *time-delayed spectra, dilute magnetic semiconductor, ZnO:Mn nanowire, excitonic magnetic polaron (EMP), spin−spin interaction, spin-phonon coupling*
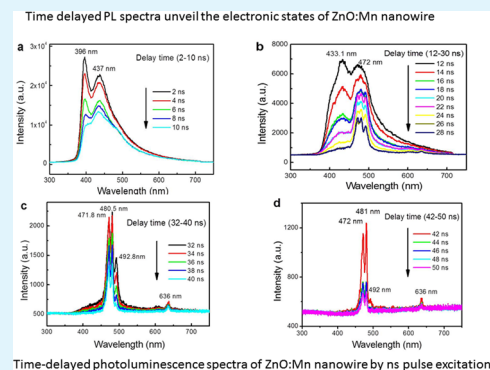
■ INTRODUCTION

Zinc oxide, a II−IV semiconductor with hexagonal wurtzite structure, has been widely applied in various fields[1] such as transducers, transparent conduction electrode, solar cells, and wide ultraviolet (UV) optoelectronic devices[2] because of its direct bandgap of 3.37 eV at room temperature and a large exciton binding energy of 60 meV. Recently, studies present that the doping of transition metal element Mn into ZnO offers a feasible mean of realizing p-type ZnO. Mn doped ZnO also has a potential to be a multifunctional material with coexisting magnetic, semiconducting and optical properties,[3−7] which makes a fine way to tune the bandgap for UV detector and light emitters. Moreover, it generates a new kind of ZnO material-diluted magnetic semiconductor (DMS). Dietl et. al[8] predicted that the transition temperature T_c in p-type ZnO DMS will be greater than 300 K, which is possibly used for making various room-temperature spintronic devices.

Concerning the preparation of ZnO:Mn compounds, many techniques including pulsed laser deposition (PLD),[3] RF sputtering,[4] chemical vapor deposition (CVD),[9] sol−gel[10] and solvent-thermal method[11] have been used. Notably, their ferromagnetism depends not only on the Mn-doping concentration but also on the preparation technique and the sample processing conditions. Hence the study on the magnetic

and optical properties of ZnO:Mn nanostructures has showed some controversy so far[3−15] because of the complicated sample compositions, interface, size, and phases, whereas most of the magnetic measurement facilities can study only the mass samples in which their ferromagnetic (FM) responses were found; however, the detailed electronic states and microscopic interactions in individual ZnO:Mn nanostructures are not unveiled yet for the short of local-zone study techniques. On the basis of the spin coupling with exciton in DMS nanostructure, micro-optical techniques like Raman, photo-luminescence, and others may be used to study the magnetic exciton or the spin- or phonon-coupled exciton in DMS, and find more applications in quantum modulations.

To better understand the electronic states and optical properties of ZnO:Mn nanostructure, we prepared the ZnO:Mn nanowires with about 300 nm thickness[16] in varied dilute doping, and found the dynamic transformation of free exciton to bipolaronic exciton, the free exciton coupled with 2LO of A_1 phonon, at a rising pumping power of a fs pulse. Mn ions, even very diluted, are supposed to FM coupled with each
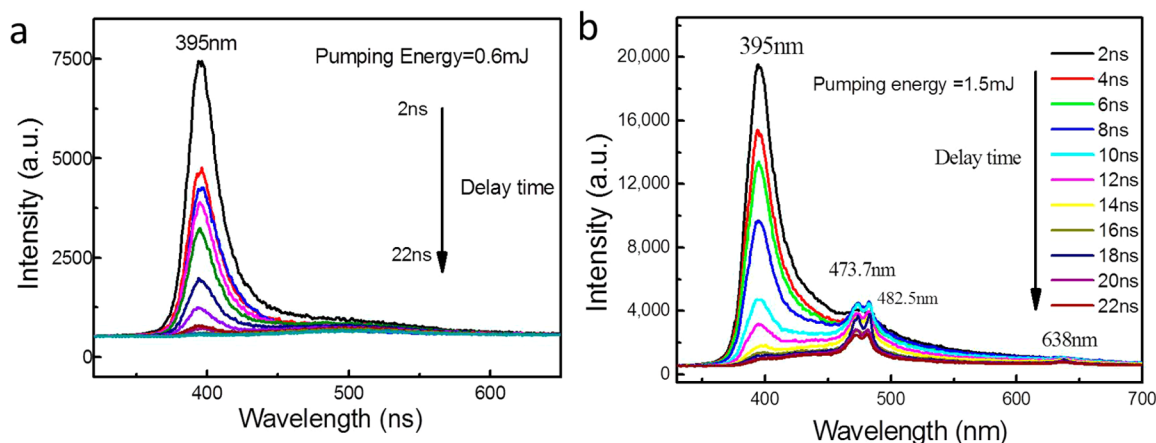
Figure 1. Delayed PL spectra of ZnO:Mn nanowires under the pump energy 0.6 mJ and 1.5 mJ, respectively. (a) At lower excitation, the spectra just show bandedge emission and a trap state emission locating at around 500 nm with 2 ns delay to 22 ns delay after the wires was excited. (b) Situation with a higher excitation energy, the bands at around 480 and 638 nm appear.

other to facilitate the exciton stability and condensation at femtosecond (fs) coherent laser excitation.[17] Clearly the happening of this phenomenon is related to the formation of highly stable delocalized exaction magnetic polarons (EMP) in DMS[18] with quasi-1D confinement effects. It is urgent and necessary to understand the density-dependent detailed electronic states and excitonic behaviors of diluted Mn-doped ZnO nanostructures, also with its dimensional effects. This understanding will facilitate the application of coherent quantum state in nanostructures. Therefore, the EMP at varied concentrations in a 1D ZnO structure with enhanced phonon coupling[16] is a good platform to study the localization or delocalization of magnetic excitons.[19]

Recently, we found that the pulse width of pump laser has significant influence on the emission wavelength of ZnSe: Mn nanostructures, which reflected the excited state population and microscopic interactions may vary for the laser pulse changes.[20] So we studied the time-delayed photoluminescence (PL) spectra of ZnO:Mn nanowire with very low Mn concentration that far smaller than 0.03%, which is slight larger than that we observed the polaronic exciton condensation(<0.01%).[17] Here a series of different d−d radiative transitions is found in their time-delayed spectra, and much clearer energy level assignments are completed. Besides this, several important phenomena are observed: (1) an anomalous weak emission peak at 636 nm is detected, which is originated from the Mn−Mn FM pair or cluster in the wire, which is verified by ab initio calculation; (2) many high levels of Mn d−d transitions are observed because of the strong p−d hybridization; (3) the lowest d-level emission shows clear LO phonon replica at high pump power, indicating polaronic exciton behavior; (4) these high levels, excited by the high power nanosecond (ns) pulse excitation, relax with spin-correlation, so they may produce coherent emission; their coherent emissions and relations to FM coupling are discussed for this 1D structure.

EXPERIMENTAL SECTION

The ZnO:Mn nanowire are produce by a CVD growth technique, the products form in the a half-sealed tube placed in a tube furnace with a mixture of ZnO (1 g), graphite (4 g), and Mn(OH)$_2$ (0.2 g) at 1000 °C for half a hour. The mixture ratio can be changed to tune the Mn doping concentration. The nitrogen is used as the carrier gas, the tube exit is open to the atmosphere. The separate nanowire array form on a zinc lump with less than 1 cm as shown in ref 17. The Mn

concentration can be modulated from 0.001% to about 1% by the ICP analysis by picking up the nanowires from the lump. Because of the existence of Zinc lump, we can propose that the nanowire is zinc rich type. During PL measurement, the Zinc lump is adhered to the sample holder, so the ZnO nanowire array can stand up in the air to be illuminated by a laser pulse of 355 nm with light spot of 1 μm in diameter. Their photoluminescence (PL) was excited by pulsed laser shots at 355 nm with pulse width 2−3 ns (Newwave Tempest model), few wires are excited, each of their PL was collected by lens and analyzed with the optical multichannel analyzer (OMA, EG&G), which was synchronized with laser pulse controlled with digital delay/pulse generator (DG535). The consecutive curves were collected with each delay time of 2 ns. The ab initio calculation is carried out with the VASP software.

RESULTS AND DISCUSSION

Time-Delayed Photoluminescence Spectra. Panels a and b in Figure 1 show the ZnO:Mn nanowire under a laser pulse of 355 nm (pulse width ∼2 ns) from the third harmonic of a Nd:YAG laser with the energy of 0.6 and 1.5 mJ, respectively. The spectral lines are collected after each 2 ns delay for different power PL detections. Under the 0.6 mJ pulse excitation, two emission peaks at 394 and 396 nm dominate at start, and a broad weak band like the first band tail show up at around 510 nm. In pure ZnO nanowire its bandedge emission from free exciton is located at 377 nm if it is prepared in a Zn-rich condition.[16] A lot of papers reported the emission of pure ZnO nanowire occurs at about 385 nm, which should be due to shallow-traped exciton in ZnO grown in O-rich environment. On the basis of the previous reports, we can know the double emission peaks and asymmetric profile near the bandedge indicate different emission origins. For the 1.5 mJ pulse excitation, the bandedge emission still dominated at around 395 nm, but its low energy side becomes more significant than that at 0.6 mJ excitation. Moreover, with the time delay two new peaks at 473.7 and 482.5 nm show up together and dominate at the late delay spectra (after 12 ns), whereas the 395 nm band dominates mainly at the early delay-time zone (before 10 ns). Between 395 and 473 nm, we did not find clear peaks shown at the different delay times. A very weak peak at 638 nm shows up at the even late delay time zone (after 18 ns).

Through the systematic examination, we can find that the PL emission of ZnO:Mn nanowires has clear Mn concentration dependent emission spectra. For example, if the Mn ions are of
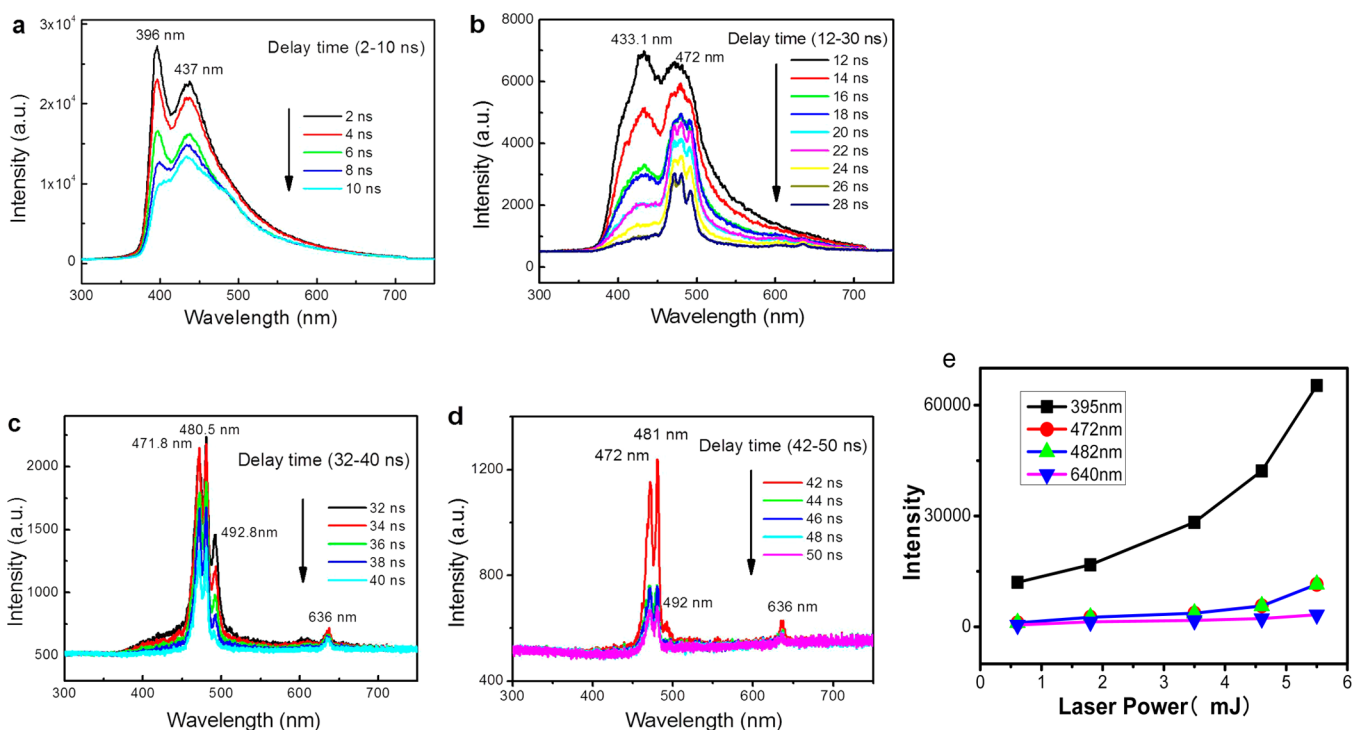
Figure 2. Time-delayed photoluminescence of ZnO:Mn nanowire under a laser pulse at 355 nm (duration 2 ns) from third harmonic of a Nd: YAG laser with the pumping energy 3.5 mJ. Each emission spectrum was collected with 2 ns time delay. (a) Observed spectra variation after the nanowire was excited within 2−10 ns delay time range. (b) Delay time gradually change from 12 to 30 ns with a 2 ns delay step, spectrum transform to different situation with Mn related peaks becoming obvious. (c, d) After a 32 ns delay, the spectra just left band around 480 nm and small peak at 636 nm, bandedge emission disappear totally. (e) Dependence of the emission intensity of various wavelength on the excitation powers.

about 0.001% in ZnO, we found two emission bands at about 376 nm (3.3 eV) and 392 nm (3.163 eV), respectively,[16] the band at 376 nm is much stronger than the band at 392 nm. If the Mn ions are >0.01%, the emission band at 392 nm becomes stronger than the band at 376 nm.[17] If the Mn ions are increased to the range of 0.03−0.3%, the band at 3.3 eV(376 nm) will disappear; the low-emission band at 392 nm gradually shifts from 392 to 405 nm as shown in Figure S1 in the Supporting Information, with gradual reduction of intensities. Moreover, we start to see the weak emission peak at 638 nm at above 0.03% doping. After about 1.5% Mn doping, we almost cannot see the bandedge emission in the range of 370−410 nm by the CW He−Cd laser excitation of 325 nm at 2−5 mW/cm^2. The two narrow peaks of 473−483 nm are shown at all Mn doping. In the synthesis of ZnO:Mn nanowire, the different furnaces have variable temperature parameters, we used varied precursor ratios. For very small doping, we can only use ICP to determine the Mn concentration, whose number in different nanowires may vary. Because the ICP technique needs to dissolve a lot of nanowires in solution, the accurate Mn concentration for individual wires could not obtained. The above results are the relative comparison in our samples.

Transition-metal-doped ZnO attracted much attention according to its importance in technology in past years. The luminescence of the ZnO crystal is strongly related to its size, structure, environment, and composition or doping; the Zn vacancy, O vacancy, interstitial structure, impurities, and adsorbed specials all can be the emission center, so many reports sometimes presented different or controversial assignment because of the difference of synthesis techniques, the Mn doped ZnO have emissions from varied bands usually in the range of 380−600 nm. Yu et al.[21] studied the influence of Mn

doing concentration in ferromagnetic ZnO nanorods obtained by thermal diffusion, found the visible emission gradual shift from 520 to 680 nm with increasing Mn concentration, though their emission band is broad because of the low crystallinity of their nanorods. Even more reports indicated the emission band in the range of 460−490 nm of Mn-doped ZnO nanoparticles,[22] which supported the emission of Mn ions in ZnO lattice. On the basis of the previous literature, it can be concluded that the perfect crystal of ZnO is important to get the pure emissions from the Mn ion in ZnO; moreover, the sample can not be laid down on the substrate. Our sample, nanowire stand up on the substrate, satisfies well the above two conditions to get good spectra.

Figure 2 shows the time-delayed PL s of ZnO:Mn nanowire under a higher laser energy of 3.5 mJ. Each emission spectrum was collected at each 2 ns delay. Figure 2a shows the delayed emission spectra in the time scale of 2−10 ns. There are two emission bands at 396 and 437 nm respectively at the early delay interval (2−10 ns), the latter did not show up at the low power excitation. In this time range the 437 nm band has a very long bandtail extended to over 700 nm, a shoulder at about 480 nm can be observed in the delay range of 8−10 ns. In the later delay intervals of Figure 2a, the above-mentioned two bands decrease with delay time, and the 396 nm band decreased much faster than the 437 nm band, then shift to 402 nm. Figure 2b shows the delayed emission spectra in the time scale of 12−30 ns. The 396 nm band already becomes a small shoulder band at about 405 nm, whereas the 437 nm band became dominant with a small redshift in the early time zone of 12−30 ns range. In the later delay time zone in Figure 2b, the 437 nm band also decreases quickly and blueshifts gradually to 433 nm, then

becomes only a broad shoulder band as the delay time approached 30 ns.

The emission band at about 470−495 nm shows up drastically in the early delay time zone of 10−30 ns, and dominates with three clear peaks in the time zone shown in Figure 2c. Three peaks at 471.8, 480.5, and 492.8 nm show up respectively and dominate. The previous two peaks at 471.8 and 480.5 nm also showed up at the 1.5 mJ excitation in Figure 1b. The third peak at 492.8 nm can appear only at high power excitation, and it disappeared at delay time of 44 ns as shown in Figure 2d, much faster than the 471.8 and 480.5 nm peaks. After 28 ns delay, the long bandtail in the long wavelength range start to disappear, and a weak peak at 637 nm and two even weak peaks at about 602 and 609 nm become clear respectively with delay time as shown in the inset of Figure 2c. The 602−609 nm peaks diminish to zero at delay 38 ns, relax much faster than the 637 nm peak does. The 637 nm peak cannot be found on the sample with Mn less than 0.03%. Figure 1d shows the emission spectra at 42−50 ns time zone. The peak at 492 nm disappeared at time delay of 44 ns, whereas the 471.8, 480.5, and 636 nm peak peaks are still present though their intensities become weaker.

On the basis of these results, the different time dependent peak occurrences and relaxations reflected their different electronic energy, carrier coupling and relaxations in the Mn incorporated ZnO nanowire, especially the energy level migration and evolution with delay time, all are short of study. Besides these, we found all the emission peaks show a superlinear intensity increasing with excitation power as shown in Figure 1e, which represented coherent radiations for related excited states. This type of behaviors is interesting and special for its 1D exciton characteristics[16,23] and spin-exciton relaxtion nature.[24,25]

The ZnO crystal excited by 355 nm produce the exciton first.[16] Some of exciton may recombine to emit light, and some of them may relax to phonon or impurities; for example, relax into the Mn ion levels when Mn is incorporated into semiconductor lattice. In fact, the fs pulse excitation on ZnO:Mn nanowire produce only free exciton and bipolaronic exciton.[17] Both of them can relax in the ps time scale. The latter one contains spin coupled phonons in c axis, and condensate into macroscopic excitonic state, because of the decoherence-free relaxation of spin-phonon coupled exciton[25] during coherent excitation. However, the identical nanowire under ns pulse excitation produces clearly different spectroscopic behavior as shown in Figures 1 and 2, because a lot of noncoherent states could be produced after ns pulse non-coherent excitation, such as the photoinduced carriers. Therefore, the intermediate states with lower energy than free exciton could be populated during relaxation.

At low-power ns pulse excitation, the emission mainly occurred at the 394 nm with broad bandtail, may partially originate from the bipolaronic exciton (BPE) at 392 nm,[17] or it could be excitonic magnetic polaron(EMP). Its long band tail indicates some other components like carriers, spins and phonons live in the long wavelength side of the BPE or EMP. The surface trapped state emission occurs at about 500 nm in Figure 1a, which is minor in air and disappears if the nanowires are dispersed in pure alcohol. This indicates the surface relaxation is present for nanowire, even minor in Zn-rich ZnO nanowire. When the photoinduced carriers encounter the Mn ions within ZnO matrix, the Mn-related emission occurs at excitation above 1.6 mJ, so the Mn ion distribution and

distances may influence their emissions. Considering no surface states, the radiation transitions via Mn ion will gradually dominate the emission spectra after long enough relaxation time and high enough populations of the states, as shown in Figures 1 and 2b.

At first, the levels of Mn ions in ZnO are not clear yet. We need to know what these emission peaks represent. The single Mn ion level in ZnO can be described by the following diagram, as previously reported in Figure 3, which is obtained by the d−
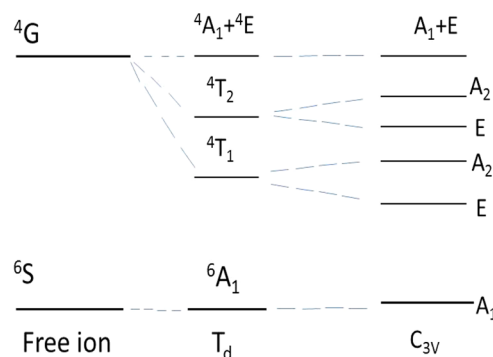

Figure 3. Diagram of Mn(II) levels in ZnO matrix. $^6A_1$ is the ground state and $^4T_1$, $^4T_2$, ^4E, and $^4A_1$ are excited states in ZnO, respectively.

d transition of Mn in the crystal filed of Zn−O lattice. Clearly the Mn ion levels should involve in the primary relaxation of exciton under the ns pulse excitation. Mizokawa et al.[26] ever used similar diagram to account for the d−d radiation transitions from the ground state $^6A_1$ to the excited states $^4T_1$, $^4T_2$, ^4E, and $^4A_1$ in ZnO are calculated to be 2.55, 2.85, 2.97, and 2.99 eV, respectively via CI energy band calculation and photoemission spectra. Their theoretical assignments are very close to the results of our delayed photoluminescence spectra; however, some interesting phenomena showed up for the properties of these levels in ZnO lattice.

The Assignment of Electronic Level of Mn Ion in ZnO. The energy levels of ZnO:Mn in the C_{3v} (wurtzite) is similar to that in T_d symmetry (zinc blende) because their crystal parameter has little difference (shown in Figure 3), only the former has a slightly lower symmetry. The theoretical levels can be used to compare with our experimental data in Figure1 and 2. For the d−d transition, the lowest level is surprisingly doublet in PL spectra, reflecting the low symmetry splitting structures of the $^4T_1 \rightarrow {}^6A_1$ transition in T_d symmetry, which is in good agreement with the two lines at 473.7 and 482.5 nm in Figure 1b, and two lines at 471.8 and 480.5 nm in Figure 2b−d. The 2 nm error in two figures should be the detector error, because the 436 nm peak in Figure 2b−d shift to 438 nm in Figure 1b with the same error. The first two lines were assigned to the transition of crystal splitting levels of E and A_2 to the A_1 in C_{3v} respectively, because they are the lowest two levels and strongest d-d transitions of Mn(II) in ZnO lattice, always show up with Mn manifestation at definite incorporation and excitation. The doublet splitting due to $T_d−C_{3v}$ transformation is detected to be 47.6 meV. The other peaks at 394−405 and 433−437 nm behave in different ways. The former always dominate in the early delay, for they have strong overlap with the polaronic excitons.[17] The latter can only happen at higher excitation power for they are at high levels and usually have too low population and probability to be observed.

10356

dx.doi.org/10.1021/am501835j | ACS Appl. Mater. Interfaces 2014, 6, 10353−10366

The 492.6 nm line in Figure 2c, d diminishes with delay times; moreover, it does not show up at low excitation in Figure 1b, indicating that it is not the intrinsic transition, but an induced one, possibly the phonon-assisted one.[27] It is located at the lower energy of 64.4 meV to the 480.5 nm peak. This 64.4 meV equals the LO A_1 mode energy of wurtzite ZnO crystal, so it represents a direct coupling between the photoinduced carrier and the excited state of one Mn spin, i.e., the magnetic polarons.[18,19] The A_1 mode occurrence and enhancement in the ZnO nanostructures after Mn doping also proved the formation of magnetic polaron.[4,17,21] under both resonant and nonresonant excitation. We cannot see it at low power because of low Mn concentration. At high power excitation, there is longer waveguide distance so more Mn ions can be excited in ZnO nanowire. This linear coupling indicates a uniform order of Mn spin in ZnO. Clearly this spin-polaron state has high relation to the spin−orbital interaction and p−d hybridization, whereas the latter can tune the spatial distribution and lifetime of Mn electronic state, then relate itself to their high d level populations and emissions.[28,29] In contrast to ZnS:Mn crystal, which gives emission only at the lowest d−d $^4T_1 \rightarrow ^6A_1$ transition at 580 nm, ZnO:Mn crystals have been found to produce complicated emission spectra at different doping concentrations, for several d orbital related high-level state emissions can be detected in the UV−visible range. Schröer et al. found p−d mixing in ZnO is about twice more than that in ZnS via first-principle calculations.[28] These experimental and theoretical results reflected the p state of O enhancing the coupling between Mn ions. So the Mn ions can be correlated with phonon- or carrier-involved polarization except spins. So the stable EMP state can form to give its emission. The d−d transition, as the localized EMP under this condition, should be also more stabilized in ZnO crystal than in ZnS. That is to say, the increased lifetime of the localized EMP or d−d transition account for their emission occurrence.

Although the 636 nm peak exists at even smaller pumping energy, we still assign the peaks at 470−482 nm to the $^4T_1 \rightarrow ^6A_1$ transition, the lowest energy transition, because (1) the 637 nm peak is very weak and narrow, which is in contrast to the clear Mn ion radiative transition in other semiconductors with clear p−d hybridization;[30] (2) the 637 nm transition always show up with the peaks around 470−482 nm,[31] but there is no occurrence at even lower Mn concentration, so it should be from a pair of Mn ions; (3) 636 nm peak present with no doublet splitting due to lower C_{3v} symmetry than T_d as $^4T_1 \rightarrow ^6A_1$ transition usually does, but double peaks show up in the range of 470−482 nm. (4) The 470−482 nm peaks can show up at even low power excitation, indicating its higher stability than other peaks, as the lowest level does. Therefore, the peaks at 470−482 nm can be reasonably assigned to the $^4T_1 \rightarrow ^6A_1$ transition. Moreover, the theoretical calculation results also supported this assignment.[26]

Concerning the $^4T_1 \rightarrow ^6A_1$ transition of Mn ion in ZnO, no well-acknowledged experimental results can be used compared with the theoretical calculations for many structural parameters modify the spectra. Bates et al.[32] presented absorption measurements of the Mn ion-doped ZnO crystals with transition energies of about 1.88, 2.95, and 3.26 eV, which were assigned to transitions from ground state $^6A_1(S)$ to excited states $^4T_1(G)$, $^4T_2(G)$, and $^4A_1/^4E(G)$ of Mn^{2+}, respectively. Because of the parity forbidden of d−d transition, the direct absorption band is not reliable to be assigned to the d levels of transition metal ions. Moreover, these assignments are not supported by any other experiments and calculations. In recent investigations, steady state PL spectra on the different ZnO:Mn nanostructures[15,33,34] have presented the peaks at 405, 435, and 470 nm individually for different samples, they are very close to our time-delayed PL peaks. These facts mean that the emissions of ZnO:Mn strongly depend on the microstructures and compositions out of varied preparation techniques. However, the authors often assign them to the defects but not to d−d transitions of Mn ions in the ZnO crystal. Clearly, defects are often present in nanostructures and relate themselves to the carrier relaxations and trappings, with strong saturation effect and preparation dependence. For no or fewer defect nanostructures like nanowire obtained by Zn-rich CVD growth,[16,17] the d−d levels, if present, may clearly manifest themselves in the time-resolved spectra, as found in this measurement. If the defect contributions are excluded as dominant luminescence sources, we can easily determine the d−d transitions and understand the electronic structure of ferromagnetic ZnO:Mn crystal via the spectral results.[3−7,9]

After the $^4T_1 \rightarrow ^6A_1$ transition in the PL spectra is determined, the band in 415−455 nm range should be assigned to $^4T_2 \rightarrow ^6A_1$ transition, with the peak position at 433 and 437 nm, correspond to the $A_2 \rightarrow A_1$ and $E \rightarrow A_1$ transitions in C_{3v} symmetry, respectively. In a typical semiconductor, like ZnS and CdS, doping Mn ion can only give emission from the lowest level. But in some semiconductors with high p−d hybridization, the high level of TM ions may emit light. It could be seen in Figure 2a, b but not in Figure 1a, b, indicating that this emission band needs high laser power to produce enough population because it is not the lowest level and has a shorter lifetime. Their occurrences are due to being located within the ZnO gap, and their lifetimes are lengthened by the enhanced p−d hybridization.[27] Their occurrences at 2−26 ns delay time and high power excitation verified this effect.

The even higher $^4A_1 \rightarrow ^6A_1$ and $^4E \rightarrow ^6A_1$ transitions in Figure 3 should be in the range of 385−415 nm as shown in Figures 1a, b and 2a. They are always the strongest band in the whole emission processes, because their energy is very close to the bound exciton and/or bipolaronic exciton[16,17] or EMPs at fs pulse excitation, especially the EMPs that exciton-coupled with spins.[7,35] Therefore, the $^4A_1 \rightarrow ^6A_1$ and $^4E \rightarrow ^6A_1$ transition zone can be easily seen because they may superpose over the excitonic states though selection-forbidden. Whether exciton or d−d transition in nanowire, they behave as excitonic in nature, but are not carriers. That is to say, the low d levels are far from exciton levels, they need longer time to populate and give emission, because these d−d transitions or d-related localized EMPs (LEMP) experience the exciton relaxation and population. If the carrier effect is dominant, the emissions in the range of 430−500 nm are stronger than the bandedge emissions[15,31,33,34] for the latter favor the defects and surface states. The cathodoluminescence spectra of ZnO:Mn film[36] seems to be in good agreement with our above assignments. Their assignment is effective for the cathode-excitation on film that may avoid many contributions from defects.

The origin of the 637 nm peak has two possibilities.[22] One is one type of defects introduced by Mn incorporation, another is the Mn−O−Mn cluster in which the Mn−Mn is FM coupled. The latter case usually relates to the concentration of doping ions, as some of the Mn ions can exist in coupled pairs.[37] These pairs could be FM coupling stabilized by the polaron-exchange interactions. For its narrow width, it is not possible to be a defect. Therefore, we assign it to the Mn−O−Mn cluster. This

Table 1. Configuration, Unit Cell, Energy Levels, Formation Energy of Lowest d−d Transition, and Mn−O−Mn Cluster in ZnO:Mn Crystal by Ab Initio Calculation
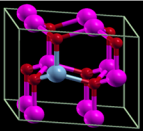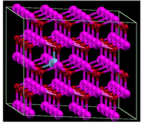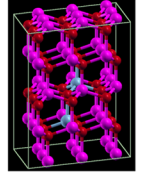
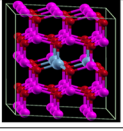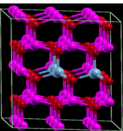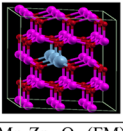| N	Mn^{2+}-doped ZnO	Description of configuration	$\Delta E(d\text{-}d)$ (eV)	Wave length (nm)	Formation energy (eV/Mn)		
					Exp (298K)	Theory(0k)	
						O-rich	Zn-rich
1	$MnZn_7O_8$	One Mn atom substitutes for Zn atom in a 2x2x1 supercell of ZnO.	2.51	494	0.797	0.248	0.437
2	$MnZn_{15}O_{16}$ (FM)	One Mn atom substitutes for Zn atom in a 2x2x2 supercell of ZnO.	2.53	490	0.792	0.243	0.432
3	$MnZn_{23}O_{24}$	One Mn atom substitutes for Zn atom in a 3x2x2 supercell of ZnO.	2.57	483	0.776	0.227	0.416
4	$MnZn_{35}O_{36}$(FM)	One Mn atom substitutes for Zn atom in a 3x3x2 supercell of ZnO.	2.685	462	0.769	0.220	0.409
5	$MnZn_{63}O_{64}$	One Mn atom substitutes for Zn atom in a 4x4x2 supercell of ZnO.	2.85	435	0.599	0.050	0.239
6	$Mn_2Zn_{34}O_{36}$(FM)	In a 3x3x2 supercell, two Mn atoms substitute for two neighbor Zn which locate at the same Zn layer.	2.18	569	0.595	0.046	0.235
	$Mn_2Zn_{34}O_{36}$(AFM)		2.797	443	0.560	0.011	0.200
7	$Mn_2Zn_{34}O_{36}$(FM)	In a 3x3x2 supercell, two Mn atoms substitute for two neighbor Zn which bond with the same S atom and locate at the up layer and down layer of the S atom respectively.	2.26	549	0.603	0.054	0.243
	AFM (Mn-S-Mn z)		2.61	474	0.579	0.030	0.219
8	$Mn_3Zn_{69}O_{72}$(FM)	In a 3x3x4 supercell, three Mn atoms substitute three Zn atoms which have same x,y coordinates.	2.77	448	0.593	0.044	0.233

Table 1. continued
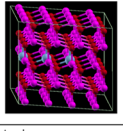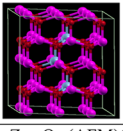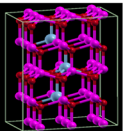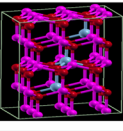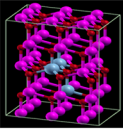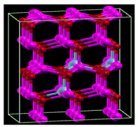
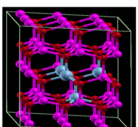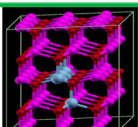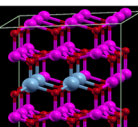| N	Mn^{2+}-doped ZnO	Description of configuration	$\Delta E(d\text{-}d)$ (eV)	Wave length (nm)	Formation energy (eV/Mn)		
					Exp (298K)	Theory(0k)	
						O-rich	Zn-rich
	$Mn_3Zn_{69}O_{72}(AFM)$		2.74	452	0.589	0.040	0.229
9	$Mn_3Zn_{33}O_{36}(FM)$	In a 3x3x2 supercell, three Mn atoms substitute three Zn atoms which form a regular triangle in a Zn layer.	2.07	600	0.622	0.073	0.262
	AFM ↑ ↑ ↓		2.278	544	0.554	0.005	0.194
10	$Mn_3Zn_{33}O_{36}(FM)$	In a 3x3x2 supercell, three Mn atoms substitute three Zn atoms which form a isosceles triangle of 120° in a Zn layer.	1.97	628	0.612	0.063	0.252
11	$Mn_3Zn_{33}O_{36}(FM)$	In a 3x3x2 supercell, three Mn atoms substitute three Zn atoms which stand in a line in a Zn layer.	1.73	714	0.608	0.059	0.248
12	$Mn_3Zn_{61}O_{64}(FM)$	In a 4x4x2 supercell, three Mn atoms substitute three Zn atoms which stand in a line in a Zn layer.	1.83	642	0.592	0.043	0.232
	↑ ↑ ↓		2.11	588	0.577	0.028	0.217
	↑ ↓ ↑		2.17	572	0.557	0.008	0.197
13	3MnZnO_p2_FM		2.22	558	0.615	0.066	0.255
	$Mn_3Zn_{33}O_{36}(AFM)(z)$		2.68	463	0.564	0.015	0.204
14	$Mn_3Zn_{33}O_{36}$	3MnZnO-zzz-p-1-FM	2.28	545	0.614	0.065	0.254
15	$Mn_3Zn_{33}O_{36}$	3MnZnO-zzz-p-2-FM	2.38	521	0.611	0.062	0.251
16	$Mn_3Zn_{33}O_{36}$	3MnZnO-zzz-p-3-FM	2.07	599	0.611	0.062	0.251

Table 1. continued

N	Mn^{2+}-doped ZnO	Description of configuration	$\Delta E(d\text{-}d)$ (eV)	Wave length (nm)	Formation energy (eV/Mn) Exp (298K)	Theory(0k) O-rich	Zn-rich
17	$Mn_3Zn_{33}O_{36}$	3MnZnO-p-FM 3x3x2	2.07	599	0.615	0.066	0.255
18	Mn4Zn32O36(FM)	In a 3x3x2 supercell, four Mn atoms substitute four Zn atoms which bond with the same S atoms.	1.83	679	0.583	0.034	0.223
19	$Mn_4Zn_{44}O_{48}$-Gamma-FM	In a 4x3x2 supercell, four Mn atoms substitute four Zn atoms, and three of them are in a line and one is in another layer.	1.8745	662	0.616	0.067	0.256
20	$Mn_4Zn_{32}O_{36}$(FM)	In a 3x3x2 supercell, four Mn atoms substitute four neighbor Zn atoms which form a diamond in a Zn layer.	1.62	764	0.633	0.084	0.273

Mn−O−Mn cluster has been found in ZnS,[38] its transition energy depend on its geometry configuration in crystal and distance to the first Mn ion, and the number of Mn ions. The nearest neighboring Mn ions have strongest exchange interactions among them to modify its energy. Its weak intensity represented that this pair has a very small population in the cross-section of the c-axis grown ZnO nanowire. It is interesting that Fe^{3+} ions in ZnO nanowire also have a very weak emission peak below the $^4T_1 \rightarrow {}^6A_1$ transition, but it is not definitely assigned.[27] From this point of view, if the pair form in ZnO, there may be FM coupling and/or antimagnetic (AFM) coupling pairs. Clearly further verification by calculation for this peak is needed.

Ab Initio Calculation on Electronic Level Energy. To know better the d level energy and band structure of ZnO:Mn, we carried out the ab initio calculation on ZnO:Mn wurtzite crystal based on density functional theory (DFT) with the local density potential approximation (LDA) exchange-correlation potential. The Vienna Ab-initio Simulation Package(VASP) code[39,40] is used for all calculation. The calculation results are typically shown in Table 1 and Figure 4a, b, the latter presented the band structure of ZnO with a supercell ($3 \times 3 \times 2$), which contain one and two Mn ions in replacement of Cd ions, respectively, for the two Mn ions are placed in the xy plane with the FM coupling. The energy levels of FM coupled $(MnO)_n$ cluster in c axis and AFM coupled cluster in different directions of wurtzite ZnO are also calculated and shown in Table 1. Although the calculation data for the energy gap of continuum bands are much smaller than the real value in all the energy band calculations of solids based on the local density potential approximation (LDA) model, the localized d level energy of

doping impurities can be calculated with high accuracy and shown in Table 1, in which the configuration, unit cell, energy, formation energy are also supplied. The excellent agreement between the calculated d−d transition energy and experiment can be understood in terms of the many-body self-energy operator,[41] which mentioned that the spatial nonlocality of the operator is the main factor of obtaining an accurate bandgap. The well-known LDA underestimate of bandgap in most II−VI and III−VI group semiconductors is induced by the different spatial scale of wave functions of valence band and conduction band, which are composed by anion-p states and cation-s states, respectively. Therefore, we get accurate transition energy due to the similar local spatial scale of d-d level. Our calculated energy for the $^4T_1 \rightarrow {}^6A_1$ transition is 462−483 nm (number 3 and 4 in Table 1), there are two Cd ions between neighboring Mn ion in the xy plane (perpendicular to the c axis). This result is very close to the calculated results by Mikozawa et al.,[26] and both of them are in good agreement with our experimental results of doublet peaks in the range of 470−485 nm. One case should be indicated for number 1, 2, if there is one Zn between nearest Mn ions, its pair energy become 490−494 nm, very close to the peak shown in Figure 2b−d. However, this peak did not show up at low power, indicate no such pair present. If the second Mn is located on the fourth or fifth Zn site along x or y direction, the lowest level of this pair may move to 435 nm for coupling as No. 5 in Table 1. This large shift due to pairing usually represent strong coupling with long-range. This situation is possible but minor population, for the peaks at around 435 nm can only be detected at high power excitation and may be related to the photoinduced magentism[42] or some high-levels of AFM coupling. Therefore, the ion distribution
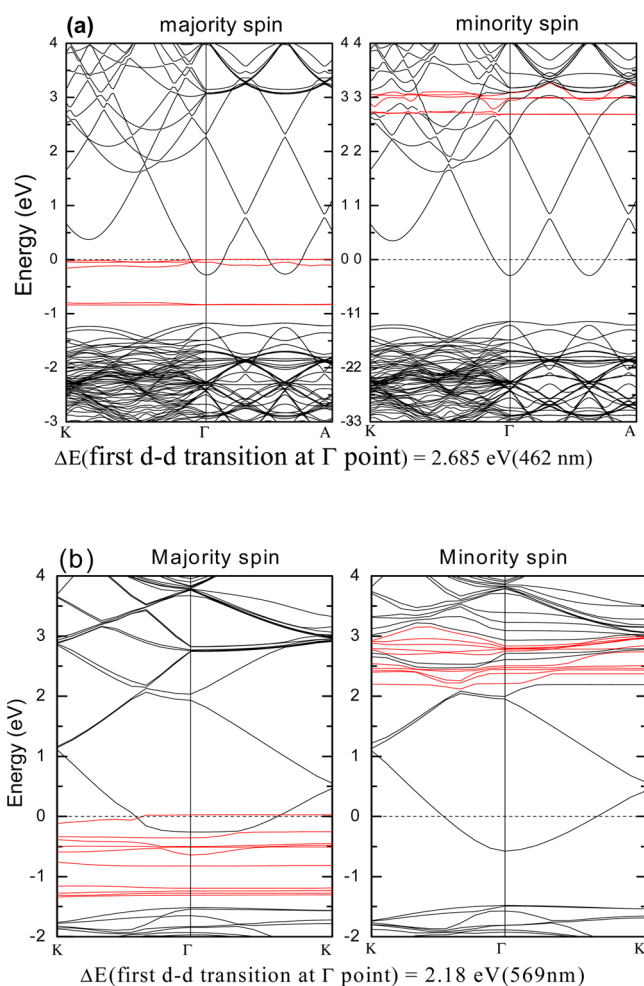
(a) majority spin   minority spin

ΔE(first d-d transition at Γ point) = 2.685 eV(462 nm)

(b) Majority spin   Minority spin

ΔE(first d-d transition at Γ point) = 2.18 eV(569nm)

Figure 4. Band structure of ZnO with a supercell (3 × 3 × 2), which contain (a) one and (b) two Mn ions in replacement of Cd, respectively. In the latter case two Mn ions are placed in the xy plane with the ferromagnetic (FM) coupling. Red lines represent d-states.

type, span, uniformity, relative location, and coupling type all influence the transition energy; moreover, enhanced covalence or p–d hybridization in TM-doped semiconductor can stabilize the high d level LEMP, which may emit light at high power excitation.[29]

In this calculation shown in Table 1, doping Mn into the ZnO lattice, the formation energy of a Mn–O–Mn cluster with single, two, three, or four did not change much for each Mn ion, and the AFM coupled cluster is usually more stable than that of the FM ones. However, it is very interesting that in our very diluted Mn-doped ZnO nanowire, the FM cluster of $(MnO)_3$ can be detected but not FM $(MnO)_2$, nor the AFM $(MnO)_n$. So this growth should be controlled by the kinetic process but not a thermodynamic one.

On the Mn–O–Mn pair energy, we calculated many configurations containing 2, 3, or 4 Mn ions as nearest neighboring ions, with FM or AFM couplings, and the results are listed in Table 1. For 2-Mn clusters, the results are 6 and 7 in Table 1, and their spectral peaks (energy) cannot be found in all the spectra. This indicates that there is no such configuration in the ZnO:Mn nanowire. For $(MnO)_3$ clusters, the results are 8–16 for more configurations. The peaks at 602–609 nm can correspond to 9, 16, and/or 17, whereas the 637 nm peak can correspond to 10 and/or 12. Such peak occurrences prove the

existence of different $(MnO)_3$ clusters in the ZnO:Mn nanowire. It must be pointed out that all the above peaks come from the FM-coupled Mn ions in the $(MnO)_3$ cluster staying in a line or plane perpendicular to the c axis of the ZnO nanowire. The clusters where all three $(MnO)_3$ located themselves along the c axis as shown by 8, 13, 14, and 15 in Table 1 have no emission peaks detected, which proves that incorporation of Mn ions into each Zn layer one by one along the c axis is difficult to complete. This is because the Mn has a larger size than Zn, and the Mn–O bond has a larger length in the xy plane than in the c axis. So this configuration would introduce stronger polarity along the c axis and deformation potential, evidenced by the enhancement of 1 LO phonon of A_1 mode in the Raman spectra of ZnO:Mn,[4,12,17,21] hence participate in the EMP.[16] These clusters, with Mn ions with FM coupling, really spectrally proved in doped ZnO nanowire, should be an origin of ferromagnetism of ZnO:Mn, which also agrees with the results (Table 1) of ab initio calculations.[43,44] Magnetic measurement on sample over M_n 0.57% really detected its weak ferromagnetism, as in previous literature.[3–7]

For the AFM coupled clusters listed in 8 and 13, their energy levels are all above 2.64 eV (470 nm). So these pairs are hard to distinguished for their locations and profiles from other single d–d transitions. In a triangle $(MnO)_3$ cluster-doped ZnO nanostructure, even Mn–Mn coupling neighboring Mn is AFM, remnant ferrimagnetism is due to them, and the surface still could be detected. For it is not applicable to determine the FM or AFM coupling between Mn ions accurately by magnetic measurement, so based on our calculation above, we can count them on their emission spectra from the d-state related transition, because the cluster of ferromagnetic coupled $(MnO)_n$ have well-defined energy values below or above the lowest energy of individual Mn ion, and easily to be detected in a perfect crystal. Our samples also have ferromagnetic responses even above room temperature, which may be related to the $(MnO)_3$-like clusters. This situation deserves further study.

Why do we choose the nearest neighboring Mns to calculate, but not the second-nearest neighboring Mn? The nearer the Mn ion locates to each other, the larger the interaction and energy change become. Because the energy of Mn–O–Mn cluster in the $x–y$ plane is smaller than that along c axis, the former population is certainly larger than that long c axis due to the inner conversion relaxation of excitons. In the energy comparison of the Mn–O clusters in FM and AFM, we find the AFM Mn–O clusters have energy higher than 474 nm, if they are present, so the peaks longer than 600 nm in wavelength cannot be assigned to AFM cluster. The second and third neighboring Mn–Mn pairing usually shows even smaller energy shift,[38] so we can ignore their contributions for this large energy shift. This spectral evidence of FM Mn–Mn pair over 600 nm in ZnO nanowire indicated its ferromagnetism. Considering the aggregation type, number, and orientation of Mn ions, optical excitation, and emission with power, one can expect the complexity of current magnetism in the ZnO:Mn nanostrucutre, even when no carriers are thought to be involved. So the microphotoluminescence technique can be a good tool to study the complicated magnetisms in different DMS materials to some extent.

Coherence Emission of d-State Emission. The lifetimes of these d–d transitions in ZnO:Mn have been obtained by the OMA with varied pulse power. Figure 5 shows the lifetimes of 474, 482, 637, and 395 nm emission with 34, 38, 31, and 6.6 ns
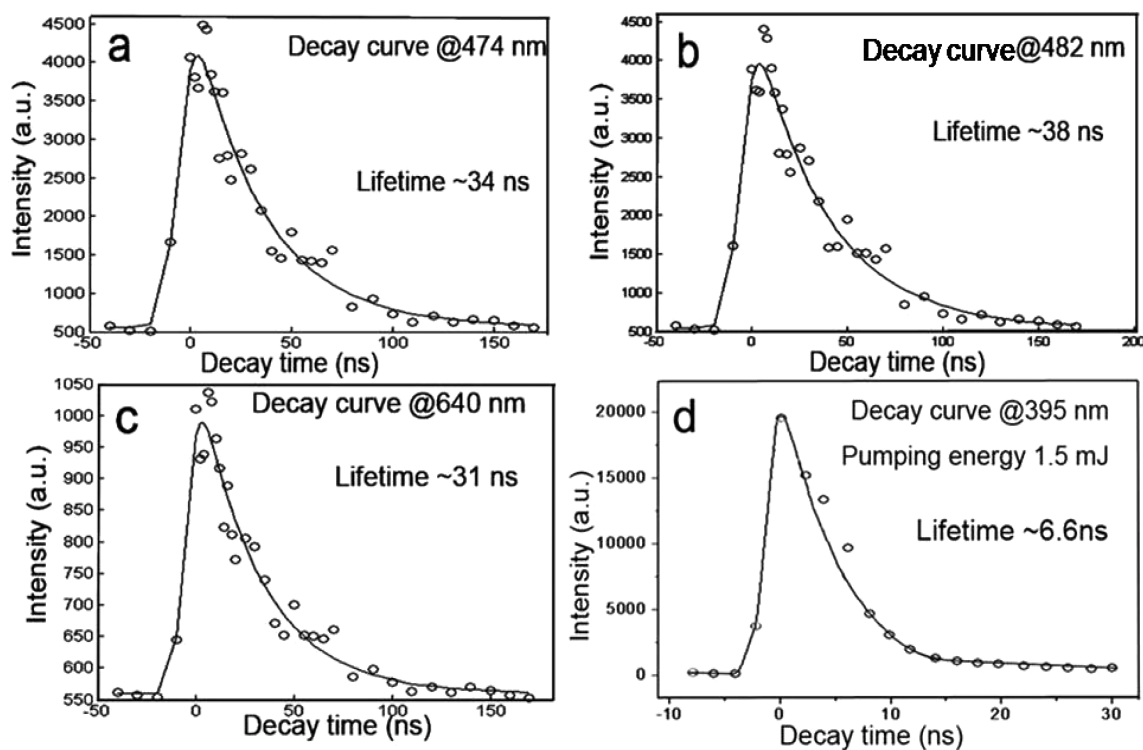
10361

dx.doi.org/10.1021/am501835j | ACS Appl. Mater. Interfaces 2014, 6, 10353–10366

Figure 5. Lifetimes of different emission at 474, 482, 640, and 395 nm under the pumping energy 1.5 mJ. The decay curve was obtained after fitting with one-exponential function with the time constant (a) 34, (b) 38, (c) 31, and (d) 6.6 ns, respectively. Single-exponential functions are shown as black lines.

respectively by 1.5 mJ pulse excitation of 355 nm. These are all long because the excitation pulse has long duration, which can excite more exciton relaxation processes with incoherent nature. From such results, many intrinsic optical properties can still be observed.[16,20]

It is reasonable that the 482 nm peak has a slightly longer lifetime than the 474 nm, because the former is the lowest level. The 640 nm peak has a short lifetime because it has a spin−spin correlation nature.[24] The 395 nm band has much smaller lifetime for its shallow trapped exciton nature. For some of d−d transitions, they form localized exciton, both its electron and hole levels are located within the gap, or the d level have no overlapping with the charge-transfer band. In ZnO:Mn, these d state occupations takes a much longer time than those electrons or holes within the conduction band or the valence band, respectively, for they are not continuous, so these states have long lifetimes. However, the dominant occupation is allocated to the free exciton, polaronic exciton, EMP near bandedge, and some d levels overlapped with above excitons, if we excite above bandgap. The latter relaxes fast.

From the lifetime data, the 640 nm peak cannot be from a defect state. If the 640 nm peak is from a defect state, its lifetime should be much longer than the d−d transition, because the lattice vibration takes part in its transition process. The fact is that it has a lifetime shorter than the $^4T_1 \rightarrow {}^6A_1$ transition (482 nm peak). Hence the 640 nm peak can be assigned to a transition of d states of $(MnO)_3$ as calculated above, and its low concentration leads to its very weak intensity. This peak rising with Mn concentration was already proved by Yu et al.[21] Concerning the 395 nm emission, it contains only short lifetime components (polaronic exciton) in picoseconds and nanoseconds within 2 ns if fs pulse is used to excite the sample.[16] Here, its 6.6 ns lifetime is related to a relaxation of

mixed states. It contains an enhanced coupling between exciton and d−d transitions or spins, including EMP, and relaxed carriers, the latter relax to the close d levels. So in contrast to the fs excitation on the coherent exciton, which give coherent behavior in relaxation, the states under ns excitation should contain multicomponents, covering many d−d transitions within the gap except bound excitons. Hence ns excitation produces more d state excitations than the fs pulse does. If we increase the power of the laser pulse to 3.5 mJ, their lifetimes change. Figure 6 shows the lifetimes of the 396, 437, 480, and 636 nm at 3.5 mJ pulse excitation. The 396 nm peak emits light with much shorter lifetime like that of free exciton and EMP, only 1.7% belongs to relaxed carriers. This change represents a more population and coherent emission of EMP at higher density.[45] The 437 nm band also shows dominant emission at about 1.2 ns, with a minor long-lifetime component of 17.6 ns. The 480 nm emission has an almost similar much shorter-lifetime component as the 437 nm band does, and a minor long-lifetime component. The second component lifetimes are longer than that under low power excitation. The minor components of long-lived transition of 43.5 ns should be the trapping states or relaxed carriers as indicated by complicated relaxation processes via in-gap states by transition metal ions doping or defects[45] with the incoherent characteristics. This is the way second components do in this system. In contrast, the dominant lifetime-shortening with powers for first component indicates that the d−d transitions in this nanowire may work like exciton to give coherent emission, and lead to spin-dependent radiation recombination processes[24] under ns pulse excitation, the emission can also be amplified with power as shown in Figure1e. This process is in significant contrast to those defects or surface states in pure ZnO nanostructures. Such lifetime shortening with density was also detected in the
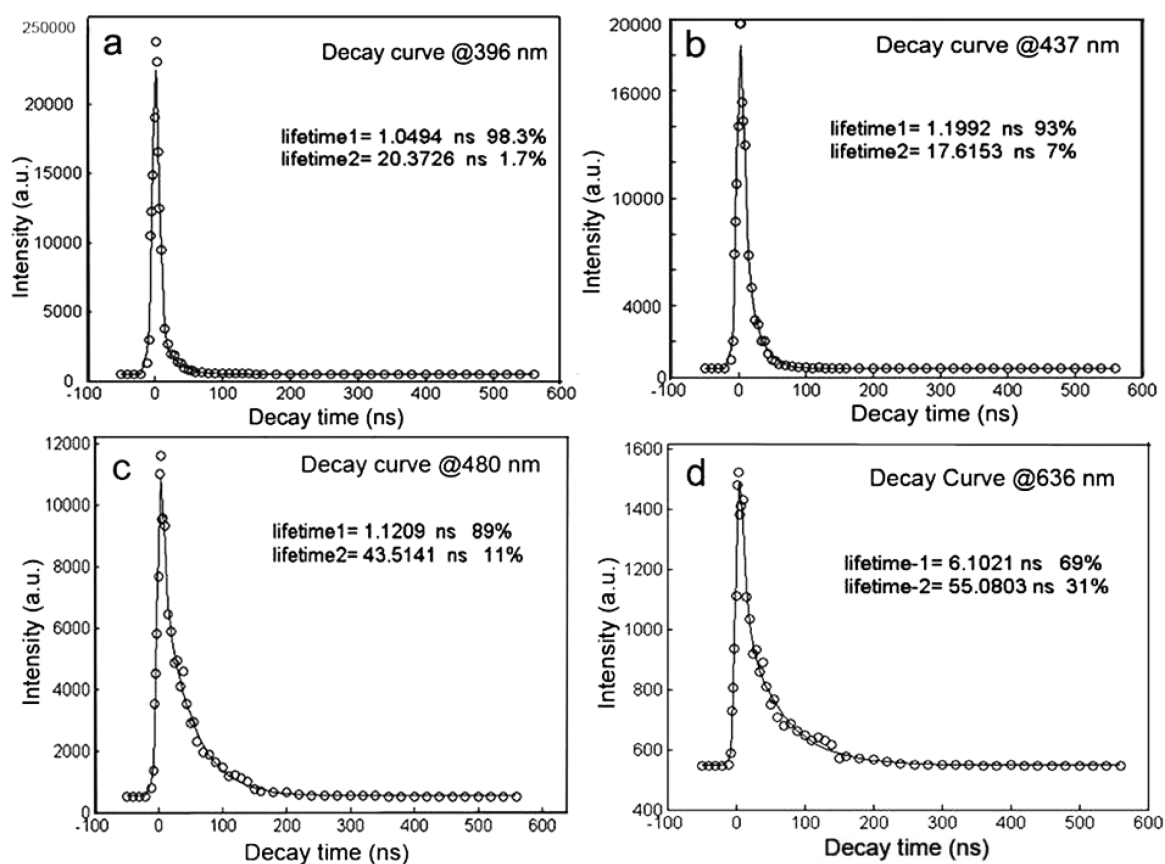
10362

dx.doi.org/10.1021/am501835j | ACS Appl. Mater. Interfaces 2014, 6, 10353−10366

Figure 6. Lifetimes of the emission at 396, 437, 480, and 636 nm under 3.5 mJ pulse excitation. The decay curves are well fit with two time-constant exponential functions. (a) Decay process at 396 nm is dominant with a much short lifetime ~1 ns (98.3%), only 1.7% with longer time ~20 ns. (b) 437 nm band also shows dominant emission at about 1.2 ns (93% part), with a minor long-lifetime component of 17.6 ns with only 7% part. (c) 480 nm emission has an almost similar much shorter-lifetime component as the 437 nm band does, and a minor longer lifetime component with 43.5 ns (11%). (d) At 636 nm, the decay process become slow with the shorter time ~6 ns (69%) and longer time ~55 ns (31%).

ZnO:Fe nanowire in ref 27. Very recently, Dey and Yarlagadda[25] indicated that decoherence-free relaxation may happen in an interacting two spin coupled to optical phonon environment. That is to say, the magnetic polaron formation may keep coherence of the spin-polaronic states because of the spin coupling. They may work for exciton magnetic polarons in DMS, for exciton to couple with two spins. Clearly, this lifetime shortening of optical d−d transition at high density accompanies the amplified emission, indicating the coherent relaxation for the LEMPs in a definite size zone.

This coherent phenomenon cannot be produced by the intrinsic individual d−d transition in doped semiconductors, but can happen by EMPs in DMS, even the localized EMPs. So the optical phonon involvement is specifically important for this type of excitation. It is wurtzite ZnO nanowire that supply enahanced strong A_1 LO phonon coupling with exciton or carriers in its 1D axis polarization.[17,21] Therefore, we can directly see the polaronic d-state emission at 492.8 nm. Its happening at high power means there is enough LO phonon population connecting two separate Mn ions with critical distance. We all know that the long-range Fröhlich interaction of carrier−phonon or exciton−phonon can be extended to longer distance, especially in a 1D waveguide like a nanowire. Therefore, the spin, exciton, and LO phonon enhancement and 1D nanowire supplied the ideal platform for the EMP and LEMP formation. Moreover, the magnetic bipolaron can also form in this 1D nanostructure because 1D structure favors their

formation.[46] The above indicated enhanced emission with lifetime shortening may be easily understood for these excitations including bipolarons.

The dense LEMPs could produce coherent relaxations in ZnO:Mn nanowire; however, their collective coherent emission cannot be easily reached because many d states coexist in the ZnO:Mn crystal, which cannot get into the same step after excitation. It is interesting that the bandedge of the ZnO nanowire can be excited to give emission from free exciton and EMP, as shown in Figure S2 in the Supporting Information. The latter could produce a coherent emission like a Bose−Einstein condensate (BEC) of bipolaronic magnetic excitons after a fs pulse excitation if no more carriers involves,[16] in which two LO phonons of A_1 mode participate in the formation of this EMP by coupling with free exciton and spin. Kavokin et al.[47] ever propose the condensation of EMP in QW; however, experimental direct verification for this condensation in QW is still not straight so far. Snoke[48] indicated the coherence behavior of magnetic exciton condensate and related emission in bilayer structure, and confessed the experimental difficulty in the BEC lasing manifestation. Moreover, the strong magnetic field plays a critical role in the BEC of magnetic excitons. This indicated their BEC realization is highly conditional in 2D structure. However, our fs excited ZnO:Mn nanowire produces efficient formation of EMP BEC at room temperature,[16] supporting the temporal condensation model requiring the longitudinal LO phonons and orientational polarization. Such

10363

dx.doi.org/10.1021/am501835j | ACS Appl. Mater. Interfaces 2014, 6, 10353−10366

1Dmagnetic exciton behavior in ZnO exactly favors the model of magnetic bipolaronic formation.[46] As is well-known, the bipolarons have been proposed to be a mechanism of superconductivity and BEC.[49] So the 1D bipolaronic excitons could be another choice for macroscopic coherent excitonic state, BEC.

EMPs propagate and polarize along the c axis, by coupling with A_1 LO phonons under fs excitation. So the ns excited exciton or carriers do the same thing to couple with LO phonons as to produce the localized EMP behavior. Then their power-dependent emissions for these different LEMP by ns excitation also undergoes the coherent relaxation processes in this Mn doped ZnO nanowire, especially the mode at 395 nm ($^4A_1-^6A_1$ transition), although ns pulse produces more carriers besides exciton and leads to more complicated excited states and relaxed processes because of complicated interactions than fs excitation does. On the basis of Kavokin's model, a giant enhancement of photoconductivity on the surface of condensate and photoinduced magnetism can be expected to be observed. From models by different authors,[48,50] the enhanced coherence of dense exciton may be related to BEC, though such measurement is not very credible to verify excitonic BEC.

Why do the collective EMPs have a much faster relaxation than the single one? The single EMP, like exciton, follows its intrinsic transition rule and usually undergoes the scattering by phonons, defects, and carriers at high temperature, giving the spontaneous radiation. Its manifestation is limited by the excitation laser pulse, especially by the broad laser pulse. All the scattering processes have been involved in its relaxation with significant magnitude as proved in the above experimental results. That is to say, many elementary excitations are excited in the broad pulse excitation. For the high power excitation of collective EMPs, their lifetime will become longer if they undergo more scattering processes as the single one does. In a favored condition with more characteristics of exciton rather carrier, the dense EMP would be coherent out of their spin–spin coupling. It is much like an exciton condensation process.[47,50] That is why collective EMPs have shorter lifetimes. For EMP condensation, the magnetic exchange plays an important role to modify their coupling and facilitate the condensation, so the ferromagnetic couplings between EMPs may be a driving force.[51] Therefore, during the condensation, the photoinduced temporal magnetism by pulse laser may also be expected in such systems with EMP condensate.

It is interesting that the 637 nm peak has a large component of a short lifetime of 6 ns, which is five times longer than that of 480 and 437 nm bands at high excitation; at the same time, it has another comparable component of a much longer lifetime of 55 ns. From this difference, we can know that the nature of 637 nm is different from that of the 480 and 437 nm peaks. The more population of short lifetime component (6 ns) than the longer one (55 ns) also support that the 637 nm peak belong to the Mn–O–Mn–O–Mn cluster in the x–y plane of ZnO lattice as shown in Table 1. The coupled spins of different Mn ions or locations in a cluster have extended time to work with polarization along c axis in ZnO nanowire, hence its population and relaxation takes more time for they are not movable. Based upon above discussion, we can know that LEMP with more TM ions need more time to couple with each other than EMP to polarize in 1D nanostructure, but the latter can collectively polarize soon to give a coherent emission out of dense excitons or condensate, although their initial energy values are also distributed in a broad range. It is seen that EMP or LEMP all

can show coherent behavior at high density, but only in different time scales. From this coherent emission and ferromagnetic cluster coexistence, we know that DMS nanowires present significant enhancement of coherent behavior for varied excitations, which may be useful for future tunable laser sources and quantum modulation via spin-light interaction.[52]

CONCLUSION

A diluted magnetic semiconductor ZnO:Mn nanowire is widely studied for its magnetic properties. Here, the energy of electronic states of doping ions are accurately determined by the time-delayed photoluminescence spectra by a ns laser pulse excitation above bandgap, are well in agreement with the theoretical calculation results. Experimental results indicate that the d–d transitions have relation to the respective localized EMP formation during the carrier relaxation. The high level d–d emission showed up unusually due to the strong p-d hybridization in ZnO:Mn nanowire and spin–spin coupling. Except for the level assignment verification, we also find the emission peak from the ferromagnetic pair of Mn ions, which may be used for the study on the magnetic mechanism of DMS in the future. Moreover, it is even interesting that the lifetime measurement by this technique proved a clear shortening of the high-density EMP and enhanced coherence in such a 1D structure, which may manifest itself in the condensation of EMP. This finding may open a new gate to studying the excition coherence and BEC of excitons, and to obtain the spin-dependent nanolaser for quantum modulation applications.

ASSOCIATED CONTENT

Ⓢ Supporting Information
Figure showing emission spectra of ZnO:Mn nanowires excited by the 325 nm He–Cd laser. This material is available free of charge via the Internet at http://pubs.acs.org.

AUTHOR INFORMATION

Corresponding Author
*E-mail: Zoubs@bit.edu.cn.
Author Contributions
Authors R.L. and L.S. contributed equally. R.L. completed all the experiments and data processing, partial writing of the manuscript; L.S. completed the calculations on the ZnO:Mn, and supplied the description of calculation results. B.Z. is the team leader, proposed the subject, and wrote the whole manuscript after discussions with many colleagues.
Notes
The authors declare no competing financial interest.

ACKNOWLEDGMENTS

REFERENCES

(1) Ozgur, U.; Alivov, Y. I.; Liu, C.; Teke, A.; Reshchikov, M. A.; Dogan, S.; Avrutin, V.; Cho, S. J.; Morkoc, H. A Comprehensive Review of ZnO Materials and Devices. *J. Appl. Phys.* **2005**, *98*, 041301−103.
(2) Tang, Z.; Wong, G.; Yu, P.; Kawasaki, M.; Ohtomo, A.; Koinuma, H.; Segawa, Y. Room-Temperature Ultraviolet Laser Emission From

Self-assembled ZnO Microcrystallite Thin Films. *Appl. Phys. Lett.* **1998**, *72*, 3270−3272.

(3) Fukumura, T.; Jin, Z.; Ohtomo, A.; Koinuma, H.; Kawasaki, M. An Oxide-diluted Magnetic Semiconductor: Mn-doped ZnO. *Appl. Phys. Lett.* **1999**, *75*, 3366−3368.

(4) Wang, J. B.; Huang, G. J.; Zhong, X. L.; Sun, L. Z.; Zhou, Y. C.; Liu, E. H. Raman Scattering and High Temperature Ferromagnetism of Mn-doped ZnO Nanoparticles. *Appl. Phys. Lett.* **2006**, *88*, 252502−252504.

(5) Sharma, P.; Gupta, A.; Rao, K. V.; Owens, F. J.; Sharma, R.; Ahuja, R.; Guillen, J. M. O.; Johansson, B.; Gehring, G. A. Ferromagnetism Above Room Temperature in Bulk and Transparent Thin Films of Mn-doped ZnO. *Nat. Mater.* **2003**, *2*, 673−677.

(6) Mi, W.; Bai, H.; Liu, H.; Sun, C. Microstructure, Magnetic, and Optical Properties of Sputtered Mn-doped ZnO Films with High-temperature Fserromagnetism. *J. Appl. Phys.* **2007**, *101*, 023904−023908.

(7) Liu, J.; Wang, K.; Yu, M.; Zhou, W. Room-temperature Ferromagnetism of Mn Doped ZnO Aligned Nanowire Arrays with Temperature Dependent Growth. *J. Appl. Phys.* **2007**, *102*, 024301−024306.

(8) Dietl, T.; Ohno, H.; Matsukura, F.; Cibert, J.; Ferrand, D. Zener Model Description of Ferromagnetism in Zinc-blende Magnetic Semiconductors. *Science* **2000**, *287*, 1019−1022.

(9) Philipose, U.; Nair, S. V.; Trudei, S.; Souza, C. F. D; Aouba, S.; Hill, R. H.; Ruda, H. E. High-temperature Ferromagnetism in Mn-doped ZnO Nanowires. *Appl. Phys. Lett.* **2006**, *88*, 263101−263103.

(10) Huang, G. J.; Wang, J. B.; Zhong, X. L.; Zhou, G. C.; Yan, H. L. Ferromagnetism of Mn-doped ZnO Nanoparticles Prepared by Sol-gel Process at Room Temperature. *Optoelectron. Lett.* **2006**, *2*, 439−442.

(11) Zhang, L. J.; Wang, J. Q.; Li, J.; Zhang, S.; Jiang, Z.; Zhou, J.; Cheng, J.; Hu, T. D.; Yan, W. S.; Wei, X. J.; Wu, Z. Y. Regulation of Magnetic Behavior and Electronic Configuration in Mn-Doped ZnO Nanorods through Surface Modifications. *Chem. Mater.* **2012**, *24*, 1676−1681.

(12) Phan, T. L.; Sun, Y. K.; Vincent, Roger.; Cherns, D.; Nghia, N. X.; Yu, S. C. Optical Properties of Mn-doped ZnO Nanowires. *J. Kor. Phys. Soc.* **2008**, *52*, 1633−1636.

(13) Liu, J. J.; Yu, M. H.; Zhou, W. L. Fabrication of Mn-doped ZnO Diluted Magnetic Semiconductor Nanostructures by Chemical Vapor Deposition. *J. Appl. Phys.* **2006**, *99*, 08M119/1−08M119/3.

(14) Roy, V. A. L.; Djurisic, A. B.; Liu, H.; Zhang, X. X.; Leung, Y. H.; Xie, M. H.; Gao, J.; Lui, H. F.; Surya, C. Magnetic Properties of Mn Doped ZnO Tetrapod Structures. *Appl. Phys. Lett.* **2004**, *84*, 756−758.

(15) Ma, X. Y.; Lou, C. X. The Dilute Magnetic and Optical Properties of Mn-doped ZnO Nanowires. *J. Nanomater.* **2011**, *2011*, 464538−464542.

(16) Zou, B. S.; Liu, R. B.; Pan, A. L.; Wang, Z. L. Lasing Mechanism of ZnO Nanowires/ Nanobelts at Room Temperature. *J. Phys. Chem. B* **2006**, *110*, 12865−12873.

(17) Liu, R. B.; Zou, B. S. Lasing Behavior from the Condensation of Polaronic Excitons in a ZnO Nanowire. *Chin. Phys.* **2011**, *20*, 47104−047104.

(18) Takeyama, S. Magnetic Polarons in Diluted Magnetic Semiconductors. In *Magneto-Optics*; Sugano, S.; Kojima, N., Eds.; Springer Series in Solid-State Sciences; Springer: New York, 2000; Vol. *128*, pp 179−209

(19) Guillaume, C. B. À. L. Free Magnetic Polarons in Three, Quasi-Two, and Quasi-One Dimensions. *Phys. Stat. Sol. (b)* **1993**, *175*, 369−380.

(20) Zhou, W. C.; Liu, R. B.; Tang, D. S.; Wang, X. X.; Fan, H. M.; Pan, A. L.; Zhang, Q. L.; Wan, Q.; Zou, B. S. Luminescence and Local Photonic Confinement of Single ZnSe: Mn Nanostructure and the Shape Dependent Lasing Behavior. *Nanotechnology* **2013**, *24* (055201), 1−12.

(21) Phan, T. L.; Yu, S. C.; Vincent, R.; Bui, H. M.; Thanh, T. D.; Lam, V. D.; Lee, Y. P. Influence of Mn Doping on Structural, Optical, and Magnetic Properties of $Zn_{1−x}Mn_xO$ Nanorods. *J. Appl. Phys.* **2010**, *108*, 044910.

(22) Viswanatha, R.; Sapra, S.; Gupta, S. S.; Satpati, B.; Satyam, P. V.; Dev, B. N.; Sarma, D. D. Synthesis and Characterization of Mn-doped ZnO Nanocrystals. *J. Phys. Chem. B* **2004**, *108*, 6303−6310.

(23) Agranovich, V. M.; Kamchatnov, A. M. Quantum Confinement and Superradiance of One-Dimensional Self-trapped Frenkel Excitons. *Chem. Phys.* **1999**, *245*, 175−184.

(24) Godlewski, M.; Yatsunenko, S.; Khachapuridze, A.; Ivanov, V. Y. Spin-dependent Recombination Processes in Wide Band Gap II-Mn-VI Compounds. *J. Alloys Compd.* **2004**, *371*, 111−113.

(25) Dey, A.; Yarlagadda, S. Polaron Dynamics and Decoherence in an Interacting Two-spin System Coupled to Optical Phonon Environment. *Phys. Rev. B* **2014**, *89*, 064311.

(26) Mizokawa, T.; Nambu, T.; Fujimori, A.; Fukumura, T.; Kawasaki, M. Electronic Structure of the Oxide-diluted Magnetic Semiconductor. $Zn_{1−x}Mn_xO$. *Phys. Rev. B* **2002**, *65*, 085209−085209−5.

(27) Müller, S. Structural and Optical Impact of Transition Metal Implantation into Zinc Oxide Single Crystals and Nanowires. *PhD thesis*, Universität zu Göttingen, Göttingen, Germany, 2009; p 134.

(28) Schroer, P.; Kriiger, P.; Pollmann, J. First-principles Calculation of the Electronic Structure of the Wurtzite Semiconductors ZnO and ZnS. *Phys. Rev. B* **1993**, *47*, 6971−6980.

(29) Kamran, M. A.; Liu, R. B.; Shi, L. J.; Zou, B. S.; Zhang, Q. L. Near Infrared Emission Band and Origin in Ni(II)-Doped CdS Nanoribbons by CVD Technique. *J. Phys. Chem. C* **2013**, *117*, 17777−17785.

(30) Benecke, C.; Gumlich, H. E. In *Diluted Magnetic Semiconductors*; Jain, M., Ed.; World Scientific: Singapore, 1991; Chapter 3, pp 85−116.

(31) Jagannatha Reddy, A.; Kokila, M. K.; Nagabhushana, H.; Rao, J. L.; Nagabhushana, B. M.; Shivakumara, C.; Chakradhar, R. P. S. EPR and Photoluminescence Studies of ZnO:Mn Nanophosphors Prepared by Solution Combustion Route. *Spectrochim. Acta, Part A* **2011**, *79*, 476−480.

(32) Bates, C. H.; White, W. B.; Roy, R. The solubility of Transition Metal Oxides in Zinc Oxide and the Reflectance Spectra of Mn^{2+} and Fe^{2+} in Tetrahedral Fields. *J. Inorg. Nucl. Chem.* **1966**, *28*, 397−403.

(33) Wang, Z.; Ma, X. Y.; Song, J. W.; Yao, J. H. Optical Properties of ZnO and Mn-doped ZnO Nano-crystals by Vapor Phase Transport Processes. *Nano-Micro Lett.* **2009**, *1*, 45−48.

(34) Hao, Y. M.; Lou, S. Y.; Zhou, S. M.; Yuan, R. J.; Zhu, G. Y.; Ning, L. Structural, Optical, and Magnetic Studies of Manganese-doped Zinc Oxide Hierarchical Microspheres by Self-assembly of Nanoparticles. *Nanoscale Res. Lett.* **2012**, *7* (100), 10−17.

(35) Okada, T.; Itoh, T. Coexistence of Bound and Localized Exciton Magnetic Polarons in $Cd_{0.8}Mn_{0.2}Te$. *J. Phys.: Condens. Matter* **2007**, *19* (186210), 1−10.

(36) Zheng, W. J.; Yoo, Y. Z.; Sekiguchi, T.; Chikyow, T.; Ofuchi, H.; Fujioka, H.; Oshima, M.; Koinuma, H. Blue and Ultraviolet Cathodoluminescence from Mn-doped Epitaxial ZnO Thin Films. *Appl. Phys. Lett.* **2003**, *83*, 39−41.

(37) Nakamura, K. Interaction of Excitonic Magnetic Polaron Pairs in Diluted Magnetic Semiconductor. *J. Phys. Soc. Jpn.* **2006**, *75*, 054712−054723.

(38) Pohl, U. W.; Gumlich, H. E. Optical Transitions of Different Mn-ion Pairs in ZnS. *Phys. Rev. B* **1989**, *40*, 1194−1201.

(39) Kresse, G.; Hafner, J. Ab Initio Molecular Dynamics for Open-shell Transition Metals. *Phys. Rev. B* **1993**, *48*, 13115−13118.

(40) Kresse, G.; Furthmüller, J. Efficient Iterative Schemes for Ab Initio Total-energy Calculations using a Plane-wave Basis Set. *Phys. Rev. B* **1996**, *54*, 11169−11186.

(41) Godby, R. W.; Schlüter, M.; Sham, L. J. Accurate Exchange-Correlation Potential for Silicon and Its Discontinuity on Addition of an Electron. *Phys. Rev. Lett.* **1986**, *56*, 2415−2418.

(42) Beaulac, R.; Schneider, L.; Archer, P. I.; Bacher, G.; Gamelin, D. R. Light-Induced Spontaneous Magnetization in Doped Colloidal Quantum Dots. *Science* **2009**, *325*, 973−976.

(43) Shi, H. L.; Duan, Y. F. Magnetic Coupling Properties of Mn-doped ZnO Nanowires: First-Principles Calculations. *J. Appl. Phys.* **2008**, *103*, 073903.

(44) Sluiter, M. H. F.; Kawazoe, Y.; Sharma, P.; Inoue, A.; Raju, A. R.; Rout, C.; Waghmare, U. V. First Principles Based Design and Experimental Evidence for a ZnO-Based Ferromagnet at Room Temperature. *Phys. Rev. Lett.* **2005**, *94* (187204), 1−4.

(45) Singh, S.; Ramachandra Rao, M. S. Optical and Electrical Resistivity Studies of Isovalent and Aliovalent 3d Transition Metal Ion Doped ZnO. *Phys. Rev. B* **2009**, *80*, 045210−045220.

(46) Kavokin, A. V.; Goupalov, S. V. Critical Conditions for 1D, 2D and 3D Magnetic-Bipolaron Formation. *Il Nuovo Cimento* **1995**, *17D*, 1527.

(47) Kavokin, A.; Gil, B.; Bigenwald, P. Collective Exciton Magnetic Polarons in Quantum Wells with Semimagnetic Barriers. *Phys. Rev. B* **1998**, *57*, R4261−R4264.

(48) Snoke, D. W. Coherence and Optical Emission from Bilayer Exciton Condensates. *Adv. Condens. Matter Phys.* **2011**, *2011* (938609), 1−7.

(49) Devreese, J. T.; Alexandrov, A. S. Fröhlich Polaron and Bipolaron: Recent Developments. *Rep. Prog. Phys.* **2009**, *72* (066501), 1−52.

(50) Dai, D. C.; Monkman, A. P. Observation of Superfluorescence from a Quantum Ensemble of Coherent Excitons in a ZnTe Crystal: Evidence for Spontaneous Bose−Einstein Condensation of Excitons. *Phys. Rev. B* **2011**, *84* (115206), 1−7.

(51) Rüegg, C.; Cavadini, N.; Furrer, A.; Güdel, H. U.; Krämer, K.; Mutka, H.; Wildes, A.; Habicht, K.; Vorderwisch, P. Bose−Einstein Condensation of the Triplet States in the Magnetic Insulator TlCuCl$_3$. *Nature* **2003**, *423*, 62−5.

(52) Echeverría-Arrondo, C.; Pérez-Conde, J.; Ayuela, A. Optical Spin Control in Nanocrystalline Magnetic Nanoswitches. *Appl. Phys. Lett.* **2009**, *95* (043111), 1−3.